Electronic Supplementary Material (ESI) for Physical Chemistry Chemical Physics.

Radical-Induced Hetero-Nuclear Mixing and Low-Field ^{13}C Relaxation in Solid Pyruvic Acid: Supplementary Information

Hana Kouřilová,[1,*] Michael Jurkutat,[1,†] David Peat,[2] Karel Kouřil,[1] Alixander S. Khan,[2] Anthony J. Horsewill,[2] James F. MacDonald,[2] John Owers-Bradley,[2] and Benno Meier[1,3,‡]

[1] *Institute of Biological Interfaces 4, Karlsruhe Institute of Technology, Eggenstein-Leopoldshafen 76344, Germany*
[2] *School of Physics and Astronomy, University of Nottingham, Nottingham, NG7 2RD, UK*
[3] *Institute of Physical Chemistry, Karlsruhe Institute of Technology, Karlsruhe 76131, Germany.*

(Dated: November 4, 2022)

CONTENTS

I. SPIN-LATTICE RELAXATION DATA

The experimental data for the ^{13}C T_1 measurements are shown in Figs. S1 and S2 together with single exponential fits.

We note that we observe ramp effects on the signal intensities. These are particularly pronounced at low evolution fields where the initial intensities ($t_{\mathrm{evo}} = 0$) appear enhanced for ^{13}C (and diminished for ^{1}H). For long evolution times ($t_{\mathrm{evo}} \gg T_1$) we find signals for ^{13}C nuclei (as well as ^{1}H) enhanced. Numerical simulations of the interaction of both nuclear reservoirs with the electron non-Zeeman during the ramp show that the effects are qualitatively reproduced by the indirect exchange mechanism described in this manuscript, i.e. by coupling with a non-nuclear reservoir whose heat capacity is not field-dependent. However, quantitatively the calculated ramp effects including exchange with the non-Zeeman reservoir account for only about one third of the observed discrepancies. Since we observe similar ramp effects in the neat sample and also for fields above 1 T, we conclude that either oxygen in our non-degassed samples is the origin or an exchange with quantized rotational states of the methyl group is responsible.

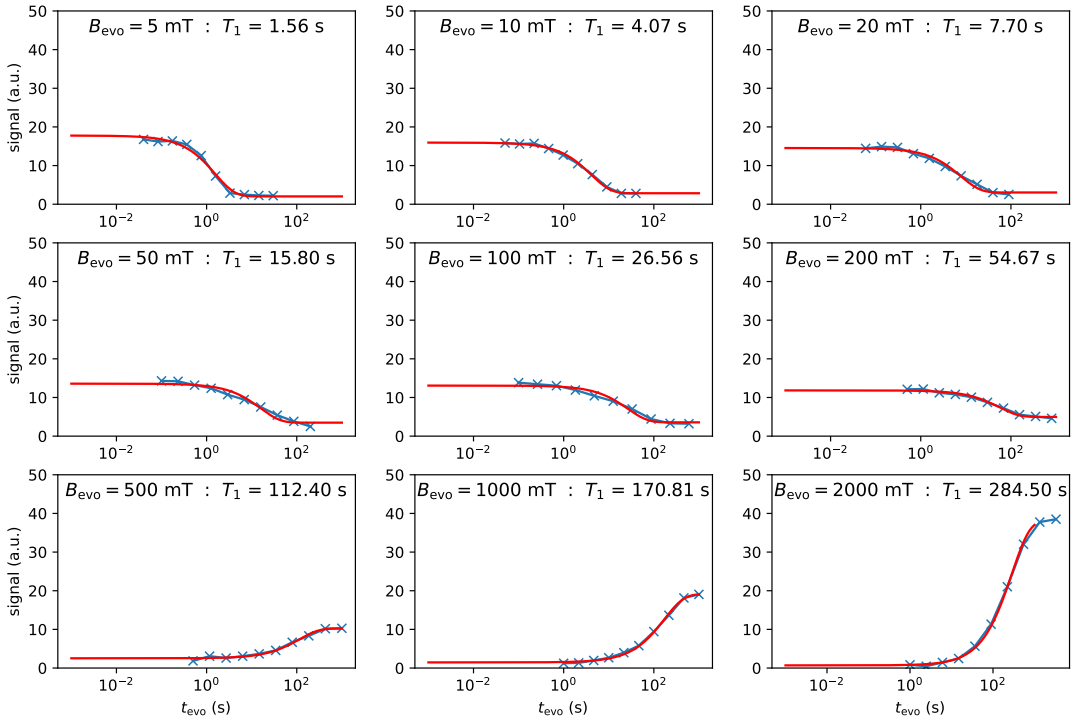

FIG. S1: ^{13}C T_1 measurements on neat PA at 4 K in different fields using polarization decay up to 200 mT and saturation recovery above.

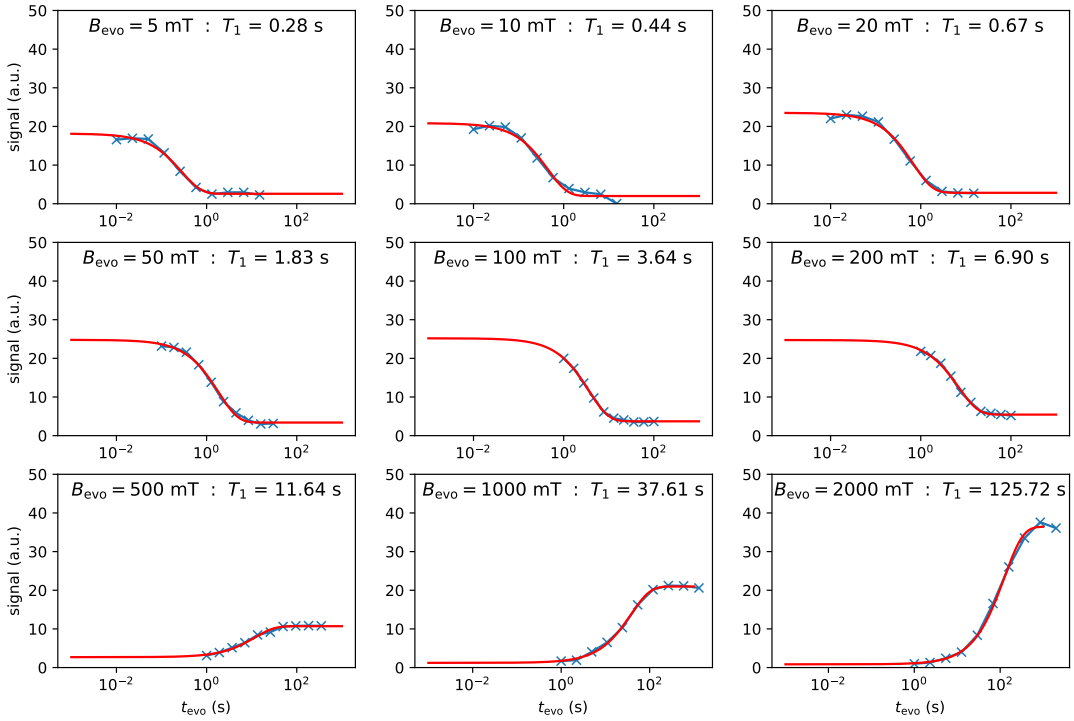

FIG. S2: ^{13}C T_1 measurements on doped PA at 4 K in different fields using polarization decay up to 200 mT and saturation recovery above.

II. THERMAL MIXING DATA

For the experiments reported here, the equilibrium ^{13}C signal at 2 T, cf. Fig. S2, is at the same time the maximum signal intensity that can be obtained via thermal mixing (TM), since the initially saturated carbon spins can at best be cooled down to the ^{1}H spin temperature, which likewise equals 4.2 K at 2 T. Therefore all TM data are normalized using the ^{13}C thermal equilibrium signal. The TM efficiency is then the ratio of the recorded ^{13}C signal and the thermal equilibrium signal.

Fig. S3 shows a comparison of thermal mixing in pyruvic acid doped with 15 mM trityl at 3 K (first row), 4.2 K (second row), 10 K (third row), 20 K (fourth row) and in neat pyruvic acid at 4.2 K (bottom row). Note that the 4.2 K data on neat and doped pyruvic acid are also shown in the main manuscript. For each sample and temperature, the first column shows relaxation data (×) recorded with a saturation recovery sequence at the carbon detection field of 2.167 T and their fit (–). This relaxation measurement was used to scale the TM data shown in the second and third column and to calculate the TM efficiency.

For doped pyruvic acid (rows 1-4 in Fig. S3) the recorded maximum TM efficiency corresponds to approximately 28% at 3 K (at 40 mT field and 0.29 s mixing delay), 40% at 4.2 K (at 20 mT and 0.01 s), 36% at 10 K (at 30 mT and 0.054 s mixing delay) and 26% at 20 K (at 100 mT and 0.054 s mixing delay).

For neat pyruvic acid (bottom row in Fig. S3), the maximum TM efficiency was 51% at 4.2 K (observed at 0 mT and 0.13 s mixing delay, as well as at 0.1 mT and 0.054 s mixing delay). As can be seen from the contour plot, our data show a local minimum in TM efficiency at 0.2 mT. This curve was reproducible. Since the absolute error of magnetic field is 2 mT, it is however likely that this data point coincides with the true zero magnetic field.

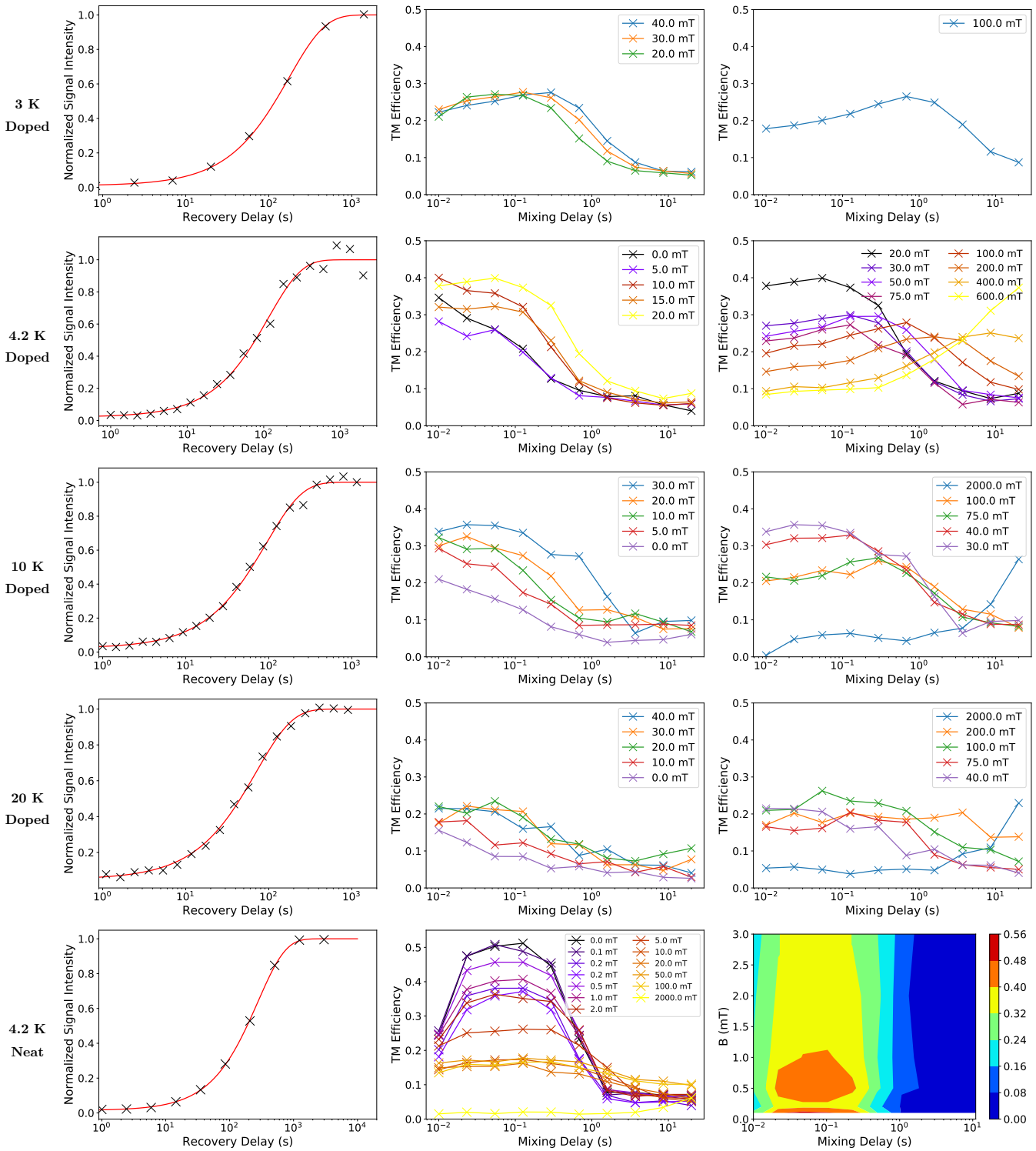

FIG. S3: Thermal mixing in doped and neat pyruvic acid at different temperatures, for details see text.

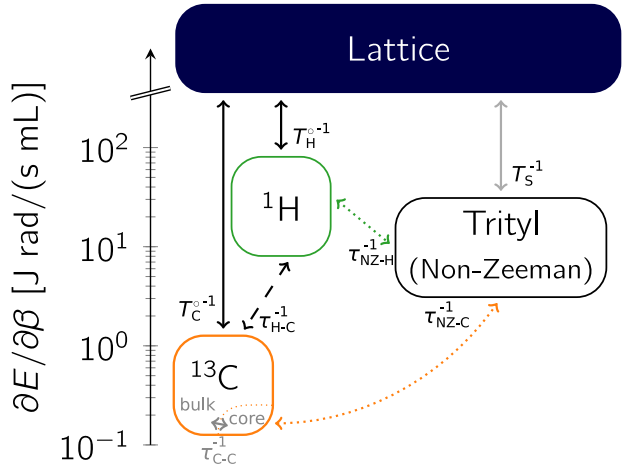

FIG. S4: Sketch of the three reservoirs coupled to the lattice and each other, with heat capacities at 20 mT as vertical axis. Carbon diffusion from the radical vicinity throughout the bulk can be included by subdividing the carbon reservoir into core and bulk as indicated in gray.

III. MULTI-RESERVOIR RELAXATION

Heat capacities

For the nuclear Zeeman reservoirs with energies E_i, with $i \in \{^1\mathrm{H},\ ^{13}\mathrm{C}\}$, and the electron NZ reservoir with E_{NZ}, the heat capacities are, respectively,

$$C_i = \frac{\partial E_i}{\partial \beta_i} = \hbar\gamma_i^2 B_0^2 N_i \frac{I(I+1)}{3} \tag{1}$$

$$C_{\mathrm{NZ}} = \frac{\partial E_{\mathrm{NZ}}}{\partial \beta_{\mathrm{NZ}}} = \hbar\gamma_S^2 H_L^2 N_S \frac{S(S+1)}{3}, \tag{2}$$

where B_0 is the applied magnetic field, γ_i is the gyromagnetic ratio and N_i is the concentration of the respective nuclear spins. The local field H_L due to spin-spin interactions is given by $\gamma_S^2 H_L^2 = (5/3)M_2$, where $M_2 = (2\pi\cdot 38\mathrm{MHz})^2$ is the second moment of the dipolar EPR line,[1] N_S is the radical concentration, and $I = S = 1/2$ is the spin of the involved species.[2] As shown in Fig. 3 (a) of the main manuscript, the Zeeman heat capacities scale quadratically with the applied field, whereas the NZ heat capacity is field-independent.

Three reservoir relaxation

The heat exchange between the three reservoirs and the lattice, illustrated in Fig. S4, is described by a set of three differential equations. These are given in matrix notation by:

$$\frac{\partial}{\partial t}\begin{pmatrix}\beta'_{\mathrm{H}}\\ \beta'_{\mathrm{C}}\\ \beta'_{\mathrm{NZ}}\end{pmatrix} = \dot{\vec{\beta}}' = \mathcal{M}\vec{\beta}' \tag{3}$$

where the $\beta'_i = \beta_i - \beta_{\mathrm{L}}$ are the respective reservoir's difference to the inverse lattice temperature β_{L} and the relaxation matrix given by:

$$\mathcal{M} = \begin{pmatrix} -\frac{1}{\tau_{\mathrm{NZ-H}}}\frac{C_{\mathrm{NZ}}}{C_{\mathrm{H}}} - \frac{1}{\tau_{\mathrm{H-C}}}\frac{C_{\mathrm{C}}}{C_{\mathrm{H}}} - \frac{1}{T_{1,\mathrm{H}}} & \frac{1}{\tau_{\mathrm{H-C}}}\frac{C_{\mathrm{C}}}{C_{\mathrm{H}}} & \frac{1}{\tau_{\mathrm{NZ-H}}}\frac{C_{\mathrm{NZ}}}{C_{\mathrm{H}}} \\ \frac{1}{\tau_{\mathrm{H-C}}} & -\frac{1}{\tau_{\mathrm{H-C}}} - \frac{1}{\tau_{\mathrm{NZ-C}}}\frac{C_{\mathrm{NZ}}}{C_{\mathrm{C}}} - \frac{1}{T_{1,\mathrm{C}}} & \frac{1}{\tau_{\mathrm{NZ-C}}}\frac{C_{\mathrm{NZ}}}{C_{\mathrm{C}}} \\ \frac{1}{\tau_{\mathrm{NZ-H}}} & \frac{1}{\tau_{\mathrm{NZ-C}}} & -\frac{1}{\tau_{\mathrm{NZ-H}}} - \frac{1}{\tau_{\mathrm{NZ-C}}} - \frac{1}{T_{1,\mathrm{S}}} \end{pmatrix} \tag{4}$$

$\tau_{\mathrm{NZ-H}}^{-1}$ and $\tau_{\mathrm{NZ-C}}^{-1}$ are the previously calculated[1] triple-spin-flip rates for proton and carbons, respectively, also displayed in Fig. 3 (b) of the main manuscript. Note that in the calculation of the carbon TSF rate $\tau_{\mathrm{NZ-C}}^{-1}$, as for protons,

we use the trityl molecular radius for the minimal distance of radical-nuclear interaction, $r_{\mathrm{ba}} = 0.7\,\mathrm{nm}$, since the diffusion barrier already for protons is inside the molecular radius. $\tau_{\mathrm{H-C}}^{-1}$ is the direct proton-carbon exchange rate that is only non-negligible at low fields ($B < 20\,\mathrm{mT}$) where it dominates the carbon relaxation, and we find it five-fold enhanced by the addition of trityl, $\tau_{\mathrm{H-C}}^{-1} \approx 5 \cdot {T_{1,\mathrm{C}}^{\circ}}^{-1}$, in that field range. The direct nuclear spin-lattice relaxation rates are given by the measurements on neat PA, $T_{1,\mathrm{H/C}}^{-1}$, and the electron $T_{1,\mathrm{S}} \approx 5\,\mathrm{s}^{-1}$ is inferred from literature data.[3]

The Eigenvalue problem of (3) can be solved numerically for each field value by determining the eigenvalues (λ_i) and corresponding eigenvectors ($\vec{v}_i$) of the relaxation matrix $\mathcal{M}$ in (4), since all entries are derived from measurements, literature data or simulations. The resulting eigenvalues λ_i (that we order as $0 \geq \lambda_1 \geq \lambda_2 \geq \lambda_3$) and corresponding eigenvectors $\vec{v}_i$ describe the three relaxation modes of the system: the slow $(\lambda_1, \vec{v}_1)$, the intermediate $(\lambda_2, \vec{v}_2)$ and the fast mode $(\lambda_3, \vec{v}_3)$.

The solution of (3) is then

$$\vec{\beta}'(t) = \begin{pmatrix} \beta'_{\mathrm{H}}(t) \\ \beta'_{\mathrm{C}}(t) \\ \beta'_{\mathrm{NZ}}(t) \end{pmatrix} = \sum_{i=1}^{3} a_i \vec{v}_i \exp(-R_i t)\,, \tag{5}$$

where the relaxation rates $R_i = -\lambda_i$ are given by the eigenvalues and coefficients a_i are determined by the initial conditions $\vec{\beta}(t=0)$.

In order to compare this three-mode relaxation to the experimentally determined single exponential decay, we can consider the combined effective relaxation rate at the time of measurement:

$$R_{\mathrm{H/C,comb}}(t = T_{1,\mathrm{H/C}}^{\bullet}) = -\frac{\dot{\beta}_{\mathrm{H/C}}}{\beta_{\mathrm{H/C}}}(t = T_{1,\mathrm{H/C}}^{\bullet}) = \frac{\sum_{i=1}^{3} R_i \cdot a_i \cdot v_{i,\mathrm{H/C}} \cdot \exp(-R_i t)}{\sum_{i=1}^{3} a_i \cdot v_{i,\mathrm{H/C}} \cdot \exp(-R_i t)} \tag{6}$$

The role of the different modes in the system's relaxation is less straight-forward than in the case of the two-reservoir relaxation.[1] In particular since here three, instead of one, inter-reservoir coupling rates ($\tau_{\mathrm{H-C}}^{-1}, \tau_{\mathrm{NZ-H}}^{-1}, \tau_{\mathrm{NZ-C}}^{-1}$) with differing field dependences contribute.

Nonetheless, the slow mode always describes the relaxation of the system as a whole with rate R_1 to the lattice temperature. All entries of the corresponding eigenvector $\vec{v}_1$ have the same sign, which signifies an overall heating or cooling of all three reservoirs at the same rate R_1 to the inverse lattice temperature β_{L}.

The other two faster modes can also involve some net heat exchange with the lattice. However, for all fields where the inter-reservoir coupling rates ($\tau_{\mathrm{H-C}}^{-1}, \tau_{\mathrm{NZ-H}}^{-1}, \tau_{\mathrm{NZ-C}}^{-1}$) are non-negligible, these modes mainly describe the internal heat exchange balancing temperature differences between the reservoirs. So both $\vec{v}_2$ and $\vec{v}_3$ have one entry with an opposite sign to the other two. This signifies that these modes cool/heat one reservoir at the expense of heating/cooling the other two. Details depend on the field-dependent reservoir exchange rates and initial conditions.

Carbon diffusion described by (3+1)-reservoir relaxation

Only a minute part of all investigated nuclei of the substrate, in our case PA, will be close enough to radical electrons to exchange energy directly. These are referred to as *core* nuclei and their resonance frequency will also be shifted by the radical's dipolar field, which renders them (partially) NMR-invisible. The observed NMR signal is dominated by *bulk* nuclei further away from the radical. These exchange only indirectly with the electron reservoir via spin-diffusion.[4]

The dipolar field around the radical is anisotropic and decreases continuously with distance, so there is no strict separation into core and bulk nuclei. Nonetheless, it is instructive to consider and compare characteristic distances from the radical. The radius around the radicals beyond which nuclei are polarized/relaxed due to the radical only indirectly, i.e., by spin diffusion, is the so-called *diffusion boundary*, r_{bo}. Another characteristic length is the *diffusion barrier*, r_{ba}, which describes the radius around the radical within which the resonance frequency of nuclei is changed by the nearby radicals' field to such an extent that spin diffusion to unaffected nuclei in the bulk is suppressed. Both these parameters were recently estimated to be smaller than the trityl molecule itself, $r_{\mathrm{bo}} < r_{\mathrm{ba}} < r_{\mathrm{trityl}}$.[5] So clearly, direct polarization/relaxation of the nuclear spins is limited to the radicals' immediate vicinity. Therefore, slow spin diffusion, whether core-to-bulk or through the bulk, can hinder both DNP as well as relaxation via trityl.

The exchange between core and bulk nuclei was recently experimentally measured for protons in another system, and successfully modelled by two coupling reservoirs.[4] In order to incorporate carbon diffusion into the model we add a fourth reservoir by dividing the carbon reservoir into core and bulk. We scale the size of the core reservoir by a

factor $\alpha \ll 1$. The bulk carbon reservoir of size $(1-\alpha)C_{\mathrm{C}}$ does not exchange energy directly with the NZ, but only with the protons, the lattice and via a spin diffusion rate $\tau_{\mathrm{C-C}}^{-1}$ with core carbons.

$$\frac{\partial\beta_{\mathrm{H}}}{\partial t} = -\frac{1}{\tau_{\mathrm{NZ-H}}}\frac{C_{\mathrm{NZ}}}{C_{\mathrm{H}}}(\beta_{\mathrm{H}}-\beta_{\mathrm{NZ}})-\frac{1}{\tau_{\mathrm{H-C}}}\frac{\alpha\cdot C_{\mathrm{C}}}{C_{\mathrm{H}}}\left(\beta_{\mathrm{H}}-\beta_{\mathrm{C,co}}\right) -\frac{\beta_{\mathrm{H}}}{T_{1,\mathrm{H}}}-\frac{1}{\tau_{\mathrm{H-C}}}\frac{(1-\alpha)C_{\mathrm{C}}}{C_{\mathrm{H}}}\left(\beta_{\mathrm{H}}-\beta_{\mathrm{C,bu}}\right) \tag{7}$$

$$\frac{\partial\beta_{\mathrm{C,co}}}{\partial t} = +\frac{1}{\tau_{\mathrm{H-C}}}(\beta_{\mathrm{H}}-\beta_{\mathrm{C,co}})-\frac{1}{\tau_{\mathrm{NZ-C}}}\frac{C_{\mathrm{NZ}}}{\alpha\cdot C_{\mathrm{C}}}(\beta_{\mathrm{C,co}}-\beta_{\mathrm{NZ}}) -\frac{\beta_{\mathrm{C,co}}}{T_{1,\mathrm{C}}}-\frac{1}{\tau_{\mathrm{C-C}}}\frac{1-\alpha}{\alpha}(\beta_{\mathrm{C,co}}-\beta_{\mathrm{C,bu}}) \tag{8}$$

$$\frac{\partial\beta_{\mathrm{NZ}}}{\partial t} = +\frac{1}{\tau_{\mathrm{NZ-H}}}(\beta_{\mathrm{H}}-\beta_{\mathrm{NZ}})+\frac{1}{\tau_{\mathrm{NZ-C}}}(\beta_{\mathrm{C,co}}-\beta_{\mathrm{NZ}}) -\frac{\beta_{\mathrm{NZ}}}{T_{1,\mathrm{S}}} \tag{9}$$

$$\frac{\partial\beta_{\mathrm{C,bu}}}{\partial t} = +\frac{1}{\tau_{\mathrm{H-C}}}(\beta_{\mathrm{H}}-\beta_{\mathrm{C,bu}})+\frac{1}{\tau_{\mathrm{C-C}}}(\beta_{\mathrm{C,co}}-\beta_{\mathrm{C,bu}}) -\frac{\beta_{\mathrm{C,bu}}}{T_{1,\mathrm{C}}} \tag{10}$$

Note that all changes from the three-reservoir description are marked in gray.

In analogy to the three-reservoir case, we can use matrix notation and the inverse temperature difference to the lattice to rewrite the set of differential equations as an eigenvalue problem:

$$\frac{\partial}{\partial t}\begin{pmatrix}\beta'_{\mathrm{H}}\\ \beta'_{\mathrm{C,co}}\\ \beta'_{\mathrm{NZ}}\\ \beta'_{\mathrm{C,bu}}\end{pmatrix} = \dot{\vec{\beta}}' = \mathcal{M}_4\vec{\beta}' \tag{11}$$

with the 4x4 relaxation matrix now given by:

$$\mathcal{M}_4 = \begin{pmatrix} -\frac{1}{\tau_{\mathrm{NZ-H}}}\frac{C_{\mathrm{NZ}}}{C_{\mathrm{H}}} - \frac{1}{\tau_{\mathrm{H-C}}}\frac{C_{\mathrm{C}}}{C_{\mathrm{H}}} - \frac{1}{T_{1,\mathrm{H}}} & \frac{1}{\tau_{\mathrm{H-C}}}\frac{C_{\mathrm{C}\cdot\alpha}}{C_{\mathrm{H}}} & \frac{1}{\tau_{\mathrm{NZ-H}}}\frac{C_{\mathrm{NZ}}}{C_{\mathrm{H}}} & \frac{1}{\tau_{\mathrm{H-C}}}\frac{C_{\mathrm{C}\cdot(1-\alpha)}}{C_{\mathrm{H}}} \\ \frac{1}{\tau_{\mathrm{H-C}}} & -\frac{1}{\tau_{\mathrm{H-C}}} - \frac{1}{\tau_{\mathrm{NZ-C}}}\frac{C_{\mathrm{NZ}}}{C_{\mathrm{C}\cdot\alpha}} - \frac{1}{T_{1,\mathrm{C}}} - \frac{1}{\tau_{\mathrm{C-C}}}\frac{(1-\alpha)}{\alpha} & \frac{1}{\tau_{\mathrm{NZ-C}}}\frac{C_{\mathrm{NZ}}}{C_{\mathrm{C}\cdot\alpha}} & \frac{1}{\tau_{\mathrm{C-C}}}\frac{(1-\alpha)}{\alpha} \\ \frac{1}{\tau_{\mathrm{NZ-H}}} & \frac{1}{\tau_{\mathrm{NZ-C}}} & -\frac{1}{\tau_{\mathrm{NZ-H}}} - \frac{1}{\tau_{\mathrm{NZ-C}}} - \frac{1}{T_{1,\mathrm{S}}} & 0 \\ \frac{1}{\tau_{\mathrm{H-C}}} & \frac{1}{\tau_{\mathrm{C-C}}} & 0 & -\frac{1}{\tau_{\mathrm{H-C}}} - \frac{1}{\tau_{\mathrm{C-C}}} - \frac{1}{T_{1,\mathrm{C}}} \end{pmatrix} \tag{12}$$

The solution is analogous to that for the three reservoir systems described above. The expected observable single-exponential carbon relaxation rate $R'_{\mathrm{C,comb}}$ is given by a weighted average of the core and bulk carbon nuclei. However, since the core nuclei are few ($\alpha \gtrsim 0$) and it is uncertain to what extent they are NMR-visible, the observed $R'_{\mathrm{C,comb}}$ corresponds to that of the bulk carbon nuclei:

$$R'_{\mathrm{C,comb}}(t=T^{\bullet}_{1,\mathrm{C}}) = \alpha\cdot R_{\mathrm{C,co,comb}}(t=T^{\bullet}_{1,\mathrm{C}}) + (1-\alpha)\cdot R_{\mathrm{C,bu,comb}}(t=T^{\bullet}_{1,\mathrm{C}}) \underset{\alpha\approx 0}{\approx} R_{\mathrm{C,bu,comb}}(t=T^{\bullet}_{1,\mathrm{C}}) \tag{13}$$

We find that a field-dependent carbon core-bulk diffusion time constant $\tau_{\mathrm{C-C}} = B\cdot 33\,\mathrm{s/T}$ describes the experimental data well. We note that the resulting carbon rate is fairly insensitive to the value of $\alpha \ll 1$. As discussed in the main manuscript, for the employed reservoir description the core-bulk diffusion rate $\tau_{\mathrm{C-C}}^{-1}$ could reflect either limited core-bulk exchange (across the diffusion barrier) or slow carbon diffusion in the bulk.

* hana.kourilova@kit.edu
† michael.jurkutat@kit.edu
‡ benno.meier@kit.edu

[1] M. Jurkutat, H. Kourilova, D. Peat, K. Kouril, A. Khan, A. Horsewill, J. Macdonald, J. Owers-Bradley, and B. Meier, "Radical-induced low-field ^1h relaxation in solid pyruvic acid doped with trityl-ox063," (2022), manuscript submitted for publication.
[2] M. Goldman, *Spin Temperature and Nuclear Magnetic Resonance in Solids* (Oxford University Press, 1970).
[3] L. Lumata, Z. Kovacs, A. D. Sherry, C. Malloy, S. Hill, J. van Tol, L. Yu, L. Song, and M. E. Merritt, Phys. Chem. Chem. Phys. **15**, 9800 (2013).
[4] Q. Stern, S. F. Cousin, F. Mentink-Vigier, A. C. Pinon, S. J. Elliott, O. Cala, and S. Jannin, Science Advances **7**, nil (2021).
[5] W. Wenckebach, A. Capozzi, S. Patel, and J. Ardenkjær-Larsen, Journal of Magnetic Resonance **327**, 106982 (2021).

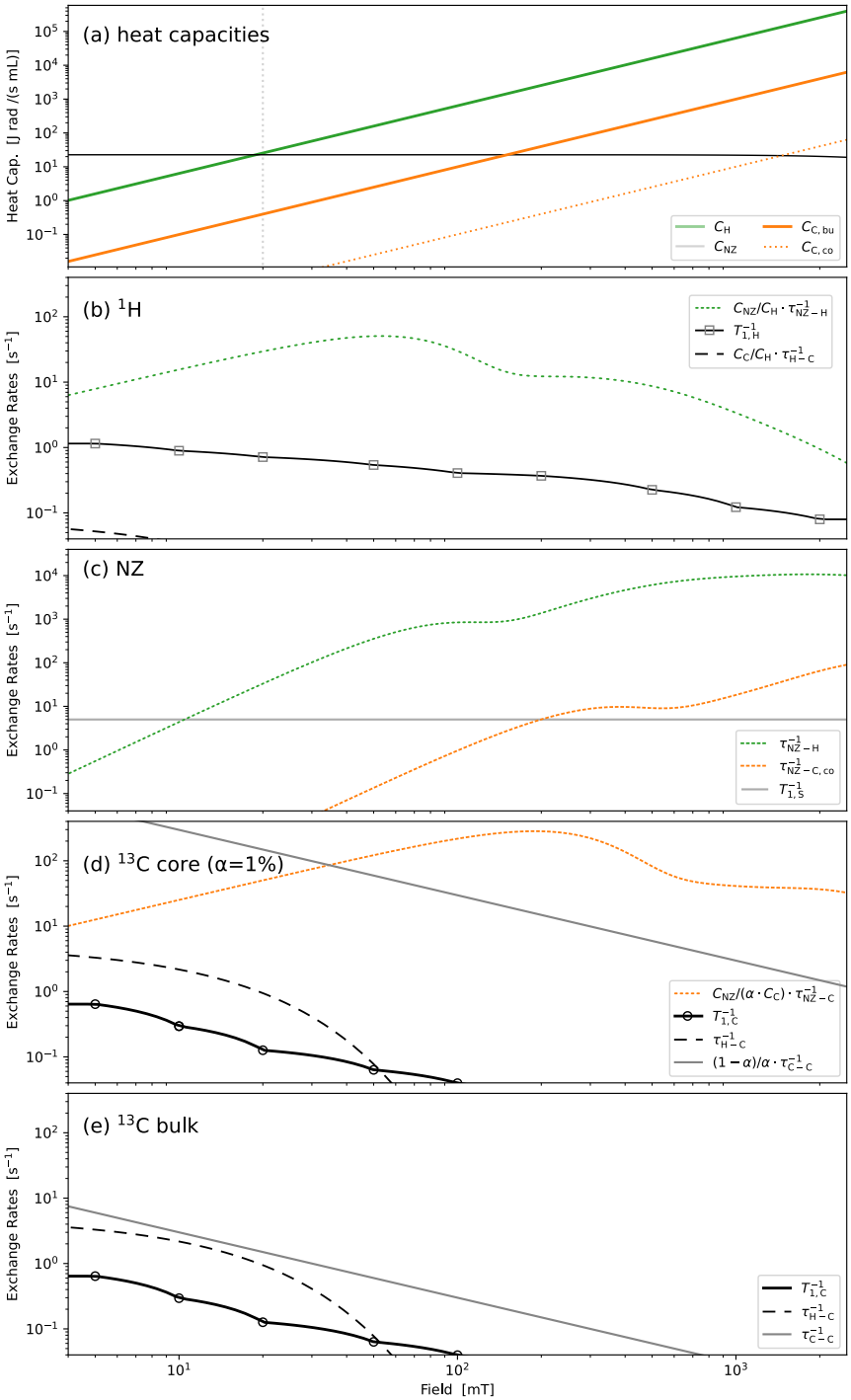

FIG. S5: Field-dependence of effective rates for reservoirs' relaxation (here displayed for $\alpha = 1\%$). (a) Heat capacities for Zeeman reservoirs grow quadratically with field, while NZ heat capacity is field independent. (b) Proton relaxation, cf. eq. (7), is dominated by TSFs at low field. As the field exceeds 20 mT, C_{NZ}/C_H goes to zero such that relaxation via NZ reservoir ($C_{NZ}/C_H \cdot {T_{1,S}}^{-1}$) diminishes and proton relaxation is increasingly via direct spin-lattice relaxation (${T_{1,H}}^{-1}$). Even at lowest fields, the effect of the direct exchange with the carbon spins ($C_C/C_H \cdot {\tau_{H-C}}^{-1}$) on protons is negligible. (c) The NZ reservoir, cf. eq. (9), at lowest field is effectively coupled to the lattice temperature. With increasing field, as ${\tau_{NZ-H}}^{-1}$ exceeds ${T_{1,S}}^{-1}$ (B >10 mT) and the proton heat capacity grows, the NZ temperature is increasingly coupled to that of the proton reservoir. (d) The carbon core spins, cf. eq. (8), at low fields are most strongly coupled to the bulk carbon reservoir via fast diffusion. Above 50 mT the core carbon spins are effectively coupled to the NZ reservoir ($C_{NZ}/(\alpha \cdot C_C) \cdot {\tau_{NZ-C}}^{-1}$) which in turn is effectively coupled to the proton reservoir. (e) The carbon bulk spins, cf. eq. (10), at low fields are coupled to the core spins via diffusion and to the proton-reservoir via direct trityl-enhanced hetero-nuclear coupling (${\tau_{H-C}}^{-1}$). The latter falls rapidly with increasing field, such that the bulk carbon reservoir's spin temperature at higher field is dominated by the diffusion from the core spins (${\tau_{C-C}}^{-1} \propto B^{-1}$), which is coupled to the NZ reservoir ($C_{NZ}/(\alpha \cdot C_C) \cdot {\tau_{NZ-C}}^{-1}$), which in turn is effectively coupled to the proton reservoir.